Multicomponent Transport of Sulfate in a Goethite–Silica Sand System at Variable pH and Ionic Strength

JOHANNES C. L. MEEUSSEN,*,†
JUTTA KLEIKEMPER,‡
ANDRÉ M. SCHEIDEGGER,§
MICHAL BORKOVEC,‖
EDWARD PATERSON,†
WILLEM H. VAN RIEMSDIJK,⊥ AND
DONALD L. SPARKS‡

Macaulay Land Use Research Institute, Craigiebuckler Aberdeen AB15 8QH, Scotland, Department of Plant and Soil Sciences, University of Delaware, Newark, Delaware 19717-1303, Waste Management Laboratory, Paul Scherrer Institute, CH-5232 Villigen, PSI, Switzerland, Department of Chemistry, Clarkson University, Potsdam, New York 13699-5814, and Department of Environmental Sciences, Sub-department Soil Science and Plant Nutrition, Wageningen Agricultural University, P.O. Box 8005, NL 6700 EC Wageningen, The Netherlands

In this work, existing models for adsorption of protons and sulfate on goethite and silica were used in combination with a one-dimensional mass-transport model to predict the transport of sulfate at variable pH and ionic strength in a goethite–silica system. The predicted multicomponent transport phenomena are discussed, and an evaluation is made of the sensitivity of the results to different input parameters. This information was used to select optimal conditions for independent experimental testing of the model. Column experiments were carried out in which solutions of known pH, sulfate concentration, and salt concentration were infiltrated into a goethite-coated quartz sand column. The agreement between the experiments and the predictions is very good, especially considering the fact that no fitting of model parameters to the actual experimental system was involved. According to the model calculations, transport behavior of sulfate in a goethite system is very sensitive to relatively small amounts of adsorbed sulfate initially present. This could be an explanation for the remaining differences between the predicted and the measured curves. It also implies that, for the application of such mechanistic models to soils, accurate information on the initial composition of the soil is essential.

Introduction

Multicomponent transport processes play an important role in the migration of both inorganic pollutants and nutrients in soil and groundwater and, thus, in the relationship between the presence of chemicals in the soil and their effects on organisms. Therefore, prediction of transport behavior as a function of soil properties can be important when evaluating the possible effects of soil contamination. Ideally, it would be possible to predict the transport rates of chemicals in a soil purely from the relevant physical and chemical parameters, using available mechanistic models for the interactions of the chemicals involved with the soil constituents. Such models are available for the adsorption of ions by soil components such as different clays, iron and aluminum (hydr)oxides, and organic matter. Although predictions with these models are unlikely to be perfect because of the variability in the chemical reactivity of soil components, they can nevertheless be very useful and provide reasonable estimations of the behavior of substances, especially of how this behavior is likely to depend on variations in soil conditions. In the case of multicomponent systems, it would be very difficult to determine such a dependence experimentally.

In this work, we investigate to what extent a multicomponent mechanistic interaction model, available from the literature, in combination with a one-dimensional convective transport model is able to predict the combined transport of sulfate and acidity in a chemically and physically well-defined system. This system consists of a goethite-coated silica sand column, which is similar to systems used in our earlier work (*1*, *2*). It is important to note that the goethite used in this column was not the same material as originally used in the literature to derive the parameters for the adsorption models. The goethite used here has a different PZC (point of zero charge) and specific surface area (*3*). The literature value for the PZC of goethite, and not the actual value for the material present in the column, was used in the model. The adsorption chemistry of silica and goethite are thus predicted using only their respective total surface areas as input.

We first used the chemical interaction model to calculate hypothetical sulfate adsorption isotherms for the column material. These isotherms were not experimentally verified. However, correct prediction of sulfate transport rates is only possible when the adsorption isotherms, including their dependency on pH and salt levels, are described accurately by the model. We subsequently used the model to calculate a set of breakthrough curves for a hypothetical column, at different pH and sulfate levels. The results of these calculations were used to select the most appropriate conditions to perform experiments that would exhibit multicomponent effects. We finally carried column experiments under these conditions and compared the resulting breakthrough curves with model simulations at the exact experimental conditions.

Model Description

The chemical adsorption models used in the calculations were taken, without any changes, from ref *4* (charging behavior of goethite), ref *5* (charging behavior of silica) and ref *6* (pH-dependent adsorption of sulfate on goethite). The adsorption models were used in combination with a one-dimensional convective transport model that was solved numerically with a mixing-cell method (*7*). The actual calculations were carried out with the computer program Orchestra (*8*). A more detailed description of the model is found in the Supporting Information.

Model Calculations

Hypothetical Adsorption Isotherms. The chemical model, defined by the reactions given in Table 1, was first used to

---

* Corresponding author phone: +44 (1224) 318611; fax: +44 (1224) 311556; e-mail: h.meeussen@mluri.sari.ac.uk.
† Macaulay Land Use Research Institute.
‡ University of Delaware.
§ Paul Scherrer Institute.
‖ Clarkson University.
⊥ Wageningen Agricultural University.

TABLE 1. Chemical Reactions Used in the Chemical Equilibrium Model

<div align="center">Solution</div>

(1) $H^+ + OH^- \leftrightarrow H_2O$	$\log K^0 = -14$	(12)
(2) $H^+ + SO_4^{2-} \leftrightarrow HSO_4^-$	$\log K^0 = 1.98$	(12)
(3) $H^+ + HSO_4^- \leftrightarrow H_2SO_4$	$\log K^0 = 0.0$	(12)
(4) $Na^+ + SO_4^{2-} \leftrightarrow NaSO_4^-$	$\log K^0 = 0.7$	(12)

<div align="center">Reactions with Goethite Surface</div>

(5) $FeOH^{1/2-} + H^+ \leftrightarrow FeOH_2^{1/2+}$	$\log K^0 = 9.2$	(4)
(6) $Fe_3O^{1/2-} + H^+ \leftrightarrow Fe_3OH^{1/2+}$	$\log K^0 = 9.2$	(4)
(7) $FeOH^{1/2-} + Na^+ \leftrightarrow FeOH_2^{1/2-} -Na^+$	$\log K^0 = -1.0$	(4)
(8) $Fe_3O^{1/2-} + Na^+ \leftrightarrow Fe_3O^{1/2-}-Na^+$	$\log K^0 = -1.0$	(4)
(9) $2FeOH^{1/2-} + SO_4^{2-} + 2H^+ \leftrightarrow Fe_2O_2SO_2^- + 2H_2O$	$\log K^0 = 19.5$	(6)
(10) $FeOH_2^{1/2+} + Cl^- \leftrightarrow FeOH_2^{1/2+}-Cl^-$	$\log K^0 = -1.0$	(4)
(11) $Fe_3OH^{1/2+} + Cl^- \leftrightarrow Fe_3OH^{1/2+}-Cl^-$	$\log K^0 = -1.0$	(1)

calculate sulfate adsorption isotherms on goethite-coated sand at different pH levels and at salt concentrations of 0.1 and 0.01 M. The calculations were done for a solid solution ratio as given in the column. The properties of the solid material and the column parameters for the hypothetical calculations were taken from ref 3. A solid matrix consisting of silica, with a specific surface area of 0.08 m² g⁻¹, and containing 0.73% (by weight) goethite, with a specific surface area of 24 m² g⁻¹ was used. The overall density of the solid material was 2.31 g cm⁻³. Combined with a porosity of 0.5, this results in 185 m² silica and 408 m² goethite/L. (Note that the column dimensions and packing density are slightly different from those of the column used in this work.)

Hypothetical Breakthrough Curves. The multicomponent sulfate adsorption model was used in combination with the one-dimensional transport model to calculate transport of sulfate, acidity, and salt ions in a goethite−silica column. First, breakthrough curves were calculated for a column equilibrated at pH 3, 4, and 5 in a 0.1 M NaCl solution. The column was infiltrated for 6 pore volumes with a 2×10^{-4}, 4×10^{-4}, and 1×10^{-3} M sulfate solution at the same pH and salt concentration. The infiltrating solution was then changed to a sulfate-free solution to leach sulfate from the column again. To illustrate the effects of the variable pH, the simulations were also performed at fixed pH.

The simulations were carried out using a system with 60 cells, resulting in a column Péclet number ($Pe = L/a$ where L is the column length and a is the dispersivity) of 150, according to the procedure reported by Herzer and Kinzelbach (9). This is lower than the Pe of 500 reported for the experimental system studied by Scheidegger et al. (1) and Meeussen et al. (2). This will result in larger effects of numerical dispersion than an experimental column. However, this is not really a problem, as the position of fronts and heights of concentration plateaus in the breakthrough curves are determined by nonlinear chromatographic effects and not by dispersion (10). This is not the case for concentration fronts that result from a change in salt concentration of the input solution. As salt is not significantly adsorbed, salt is not retarded, and there are no chromatographic effects; thus, front shapes are completely determined by dispersion (10).

To illustrate the effects of dispersion on the transport of salt and, indirectly, on accompanying ions, simulations were carried out for a column that was initially equilibrated with 6×10^{-4} M sulfate at pH 4.0 in 0.1 M NaCl. This column was infiltrated with a similar solution but now is in 0.01 M NaCl. After complete breakthrough, the input solution was replaced again with the initial solution at 0.1 M NaCl. The simulations were carried out at discretizations of 60, 120, 240, and 600 cells. According to the aforementioned procedure, this results in numerical dispersivities for unretarded fronts that are equivalent to column Pe values of 150, 300, 600, and 1500. The value of 600 is in the same range as the column Pe of

500, as reported for the experimental system studied by Scheidegger et al. (1) and Meeussen et al. (2).

Simulations of the Column Experiments. For the simulations of the column experiments carried out in this work, exactly the same model was used as for the hypothetical system. The system conditions, initial pH, salt concentrations, and column characteristics (length, diameter, porosity, amount of column material; see Experimental Section) were adjusted to conform to those in the experiments. A spatial discretization of 150 cells was used. Combined with a time step of 1/750 pore volume, this results in a numerical dispersivity equivalent to a Pe of 375 for an unretarded front and 300 for a strongly retarded front. This is close to the Pe of 300 as measured for the experimental column.

To demonstrate the effects of relatively small amounts of sulfate present in the column before the start of an experiment, we have also included model calculations for a column that initially contained the amount of sulfate that would remain after leaching with sulfate-free solution for 30 pore volumes.

Experimental Section

The preparation of the column material was carried out according to the method reported more extensively by Scheidegger et al. (3). A detailed description of the experimental methods is found in the Supporting Information.

Results and Discussion

Hypothetical Sulfate Adsorption Isotherms as a Function of pH and Salt Concentration. The adsorption isotherms of sulfate at the combined goethite−silica surface were calculated at a range of pH values and at two salt concentrations (Figure S.1 in the Supporting Information). The pH-dependent sulfate adsorption model, as embodied by reaction 9, Table 1, was originally derived from measurements in 0.1 M KCl (6). The salt dependency shown here is purely predicted from the assumed reaction mechanism and the model for the salt-dependent charging behavior of goethite. The curves clearly demonstrate the strongly nonlinear adsorption of sulfate and its dependency on both the pH and the salt concentration. The calculated decrease in sulfate adsorption at the higher salt concentration is the overall result of several processes: first, the formation of sulfate complexes with salt ions (reaction 4, Table S.1 in the Supporting Information); second, the competition of salt ions with sulfate for binding sites, and finally, and most importantly, the effect that the salt concentration has on the relationship between surface charge and surface potential.

To describe the pH dependency of sulfate adsorption, the model calculates the amount of adsorbed protons and sulfate at each combination of pH and dissolved sulfate concentration. Upon changes in pH and sulfate, the model is thus able to calculate the accompanying changes in

adsorbed concentrations of protons and sulfate. As the transport rates of solutes are determined by changes in their adsorbed concentration relative to changes in their dissolved concentration, correct calculation of both concentrations is essential for transport calculations.

Hypothetical Breakthrough Curves for Sulfate and pH. *Initial pH 3.* The calculated curves show that, for all sulfate concentrations, initial breakthrough of sulfate occurs with a sharp front during which the concentration increases to the level of the input solution (Figure S.2a in the Supporting Information). The higher concentrations appear to travel faster, which is caused by the nonlinearity of the sulfate adsorption. The accompanying pH curve (Figure S.2b in the Supporting Information) shows that the adsorption of sulfate at the first front results in a temporary increase of the pH, which is the result of net proton adsorption upon the adsorption of sulfate. The magnitude of the pH increase depends on the sulfate concentration but is relatively small in all cases. As the amount of adsorbing sulfate ions is of the same order of magnitude as (but not necessarily equal to) the amount of adsorbing protons, the pH increase depends on the pH and sulfate concentration of the column and the infiltrating solution.

Upon switching the infiltrating solution to the one without sulfate, after 6 pore volumes, sulfate leaches from the column with a diffuse front. A rapid initial decrease in concentration is followed by a very gradual further decrease. At the same time there is a temporary small decrease in the pH of the effluent, which is the result of the concomitant desorption of protons (Figure S.2b in the Supporting Information). Although the sulfate concentration in the column effluent is apparently close to 0 after 18 pore volumes, this does not imply that leaching of sulfate is complete here. Because of the nonlinearity of the sulfate adsorption (Figure S.1), about 50% of the sulfate is still present (in adsorbed form) in the column at the end of the simulation. Complete removal of sulfate from a column by simply flushing with sulfate-free solution will take a very long time as the retardation of sulfate becomes stronger with decreasing concentrations (*1, 10, 13*).

The combination of a steep infiltrating and a diffuse leaching front are typical for nonlinear adsorbing substances in a one-component situation (*1*). Although the pH−sulfate system studied here is determined by two independent components, the changes in pH are so minimal that they do not noticeably affect sulfate transport. As a result, the system behaves effectively as a one-component system with only the sulfate concentration as a variable. This aspect is further illustrated by the fact that, in the system with fixed pH, the sulfate breakthrough curves are virtually identical (Figure S.2b in the Supporting Information).

Initial pH 4. The simulations were repeated at an initial pH 4 for the column and the infiltrating solution. As in the previous calculations, the initial breakthrough of sulfate occurs with a steep front, the velocity of which depends on the sulfate concentration of the infiltrating solution (Figure S.3a in the Supporting Information). However, the breakthrough curve is now clearly split into two fronts. This agrees with chromatographic theory, which predicts that the number of retarded fronts equals to the number of adsorbing components in the system (*13*). The first front travels faster than the one at constant pH, and the second front travels significantly slower.

In the accompanying pH breakthrough curve, we can see for all sulfate concentrations that at the first front the pH increases from 4 to about 5.7 (Figure S.3b). The different shape of the pH curve in the case of solution with the lowest sulfate concentration is caused by the fact that the front is composed of a diffuse and a sharp part. Just as in a one-component situation, the diffuse part only becomes visible when it moves faster than a directly trailing sharp one. At the

second front, the pH returns to the value of the infiltrating solution. This temporary pH increase in the column effluent relative to the input solution provides the protons necessary for the adsorption of the amount of sulfate that is in equilibrium with the input solution at pH 4.

After 6 pore volumes, the input solution was changed to one without sulfate. The sulfate leaching curves are diffuse, as was the case at pH 3. Again the curves split into two fronts, which are easy to identify in the pH curves. Here the pH decreases clearly at the first front and slowly returns to its original value at the second front.

In comparison with the pH 3 system, there are now clear multicomponent characteristics. This is caused by the fact that both the dissolved proton and the sulfate concentrations are now of comparable magnitude. Apart from splitting the curves into two fronts, another effect of this multicomponent behavior is that, at variable pH, complete breakthrough of sulfate takes significantly longer than at constant pH. Complete breakthrough at calculated pH also takes longer at pH 4 than at pH 3, although sulfate adsorption is stronger at the lower pH.

Initial pH 5. At an initial pH 5 of the column and of the infiltrating solution (Figure S.4a), the infiltration curves for sulfate and pH are again split into two fronts, although this is barely visible in the sulfate curves. The first front is retarded very little, and initial breakthrough occurs with a steep front shortly after 1 pore volume. However, complete breakthrough now takes about 25−30 pore volumes. At the first front, the pH increases with a steep front from 5 to around 6, depending on the sulfate concentration (Figure S.4b in the Supporting Information). At the second front, the pH returns, again with a steep front, to its original value.

Upon leaching of sulfate, which in this case starts when the input solution is changed to a sulfate-free one after 32 pore volumes, the sulfate concentrations return to zero in the form of a diffuse front. The accompanying pH curve shows that both curves are split up in two fronts. At the first front, the pH decreases by 0.5−1 unit and returns to its initial value with a diffuse second front. Although sulfate adsorbs much less strongly at pH 5 than at pH 4 (Figure S.1 in the Supporting Information) and as a result can be expected to travel faster, at variable pH complete breakthrough of a sulfate solution takes much longer than at pH 4 or pH 3.

Although the system is theoretically a multicomponent system, the expected separation into different fronts is not obvious in the sulfate breakthrough curves. This is caused by the fact that at pH 5 the dissolved sulfate concentrations are much higher than the proton concentrations. As a result, the sulfate behavior affects the proton behavior (Figure S.4a in the Supporting Information), but there is little feedback of the pH on the dissolved sulfate concentrations (Figure S.4b in the Supporting Information). However, although not visible in the breakthrough curves, there still is a large effect of the pH on the adsorbed sulfate concentration, which increases nearly 2-fold at the second front where the pH returns from around 6 to 5. Complete saturation of the column with sulfate at constant pH takes only several pore volumes, while at variable pH this will take 25−35 pore volumes.

Changing Salt Concentration. Because the salt concentration can affect the adsorption of other ions, such as protons or sulfate, transport of salt concentrations can cause (un-retarded) transport of accompanying reactive ions. As the salt concentration is an extra variable, the system now has become a three-component system. In the pH and sulfate breakthrough curves, three fronts can be identified (Figure S.5A,B in the Supporting Information). In the sulfate curve, the concentration decreases to a fraction of its initial value at the first front. This coincides with the breakthrough of the

unretarded salt concentration. The magnitude of this decrease depends on the dispersion level, and at low dispersion levels the concentrations approach zero. After this unretarded front, the concentration immediately returns to almost its initial value at the second front. This return is fully completed during the third front after nearly 3 pore volumes. As a result of the decreased salt concentration, the amount of sulfate adsorbed by the column increases (Figure S.1 in the Supporting Information). This extra sulfate is used from the input solution and results in the temporary decrease of the sulfate concentration in the output solution.

When the input solution is changed to a lower salt level, after 6 pore volumes, an almost mirror image pattern evolves. In this case, the sulfate concentration sharply increases at the first front and returns immediately to almost its original value at the second front. This return is completed during the third front.

In the pH curve we can also identify the three separate fronts. During the first front, after almost exactly 1 pore volume, the pH decreases sharply. The pH immediately increases to more than its initial value at the second front and returns to its original value with a third front, which is complete within 3 pore volumes.

From these hypothetical breakthrough curves, it follows that in order to show the mutual interaction between pH and sulfate most clearly, with visible multicomponent effects in the sulfate as well as the pH curve, the dissolved sulfate concentration has to be of the same order of magnitude as the proton concentration. The calculations at pH 5 show that, even though there are no multicomponent effects visible in the sulfate curves, multicomponent phenomena do occur and are responsible for the fact that it takes around 30 pore volumes before the pH is in equilibrium with the input solution again.

The hypothetical breakthrough curves for systems with changing salt concentrations show that unretarded transport of salt can cause unretarded breakthrough of accompanying ions of which the adsorption is salt dependent. Dispersion can have large effects on the form of unretarded fronts. Accurate prediction of these curves depends critically on correct description of the salt dependency in the adsorption models and on the correct dispersion level.

To illustrate the effects of different sulfate–proton concentration ratios and of changing salt concentrations, we decided to conduct the following experiments.

Column Experiments. *Initial pH 4.74.* The first experiment was carried out with a column equilibrated at pH 4.74 in 0.1 M NaCl, which was infiltrated with a 1085 μM sulfate solution until complete breakthrough (Figure 1A). After 20 pore volumes, the infiltrating solution was changed to one without sulfate. The predicted sulfate and pH breakthrough curves were calculated using the initial chemical composition of the column and of the input solutions as input parameters. The conditions in this experiment are comparable to those applied for the hypothetical breakthrough curves at pH 5. According to the predictions, there will be little visible effect of the varying pH on the sulfate breakthrough but a significant effect on adsorbed sulfate and feedback of sulfate transport on the pH.

The breakthrough curve for sulfate shows rapid initial breakthrough. At first sight, breakthrough appears to be complete within about 2 pore volumes. Upon changing the input solution to one without sulfate, a rapid initial decrease of the sulfate concentration is followed by a diffuse front during which the sulfate concentration decreases to virtually zero. This asymmetric behavior, with a steep front upon infiltration and a diffuse front upon leaching, is typical for strongly nonlinearly adsorbing substances such as sulfate.

The measured sulfate curve agrees very well with the predicted curve. However, the separation of the curve into
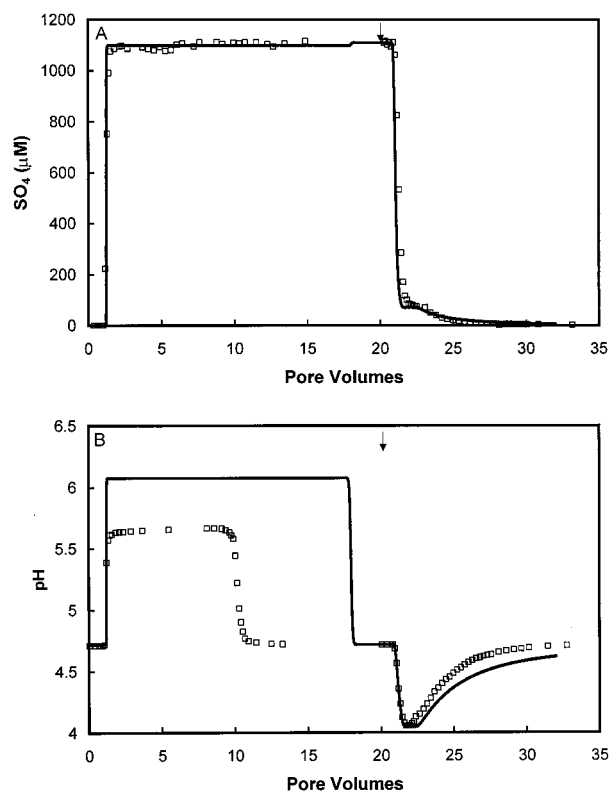

FIGURE 1. Measured and simulated breakthrough curves for a column equilibrated without sulfate at pH 4.74 and infiltrated with a 1085 μM sulfate solution at pH 4.74. After 20 pore volumes, indicated by the arrow, the input solution was replaced with a sulfate free solution of the same pH. (A) Total dissolved sulfate. (B) pH.

two fronts, which is calculated and is in line with multi-component chromatographic theory (*10, 13*), is too small to be visible in the measurements.

In the accompanying pH curve, the two separate fronts are much easier to recognize (Figure 1B). At the first front, the pH increases from 4.74 to about 5.5 and remains at this level until it returns to the pH of the input solution at the second front. After this front, the column is in equilibrium with the input solution. Although the predictions also show this temporary rise in the pH, the measured pH increase is smaller, and the plateau is significantly shorter than predicted.

When the infiltrating solution is changed to the sulfate-free solution, after 20 pore volumes, the pH decreases sharply at the first front, which coincides with the first sulfate front. Without a clearly recognizable plateau of constant pH value, the pH gradually increases again to its initial value during the second diffuse subfront.

Here the model appears to predict the pH curve very well, although during the last part of the diffuse curves especially there are differences between measured and predicted curves. In this part of the desorption curve, the model calculates sulfate adsorption at concentrations that are very low relative to the concentrations that were originally used to derive the sulfate adsorption model (*6*).

The breakthrough curves for the experiment at the lower sulfate concentration of 384 μM are very similar, although the resulting pH changes are now somewhat smaller due to the smaller amounts of adsorbing and desorbing sulfate. The sulfate breakthrough curve is predicted accurately (Figure 2A), and again the largest discrepancy appears to be in the predicted height and length of the pH plateau between the first and second fronts (Figure 2B). However, the general features of the pH curve are described well.

Initial pH 3.71. According to the hypothetical model predictions, the separation of the breakthrough curves in
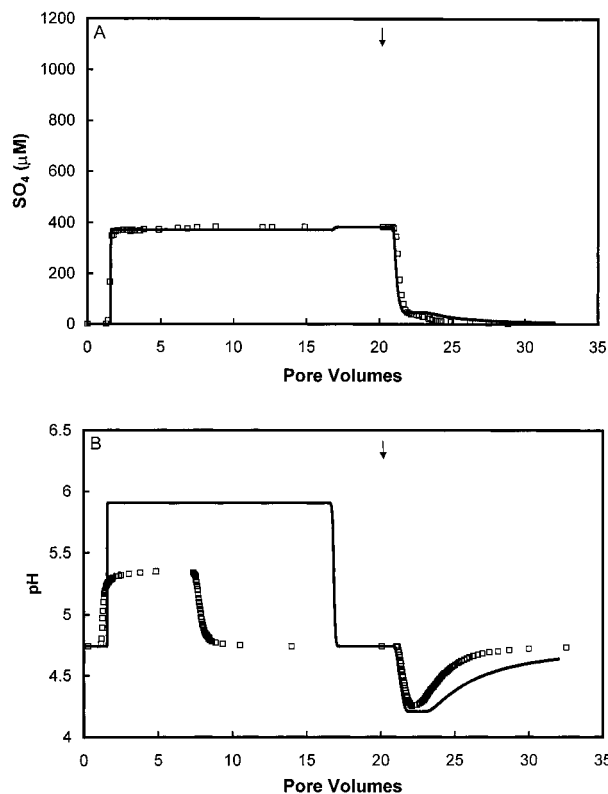
FIGURE 2. Measured and simulated breakthrough curves for a column equilibrated without sulfate at pH 4.74, infiltrated with a 384 μM sulfate solution at pH 4.74. After 20 pore volumes, indicated by the arrow, the input solution was replaced with a sulfate free solution of the same pH. (A) Total dissolved sulfate. (B) pH.

FIGURE 3. Measured and simulated breakthrough curves for a column equilibrated without sulfate at pH 3.71, infiltrated with a 1110 μM sulfate solution at pH 3.71. After 6 pore volumes, as indicated by the arrow, the input solution was replaced with a sulfate free solution of the same pH. (A) Total dissolved sulfate. (B) pH.

two fronts will be easier to recognize in the pH as well as the sulfate curves at a lower pH. We therefore conducted another experiment at pH 3.71. The proton concentrations are now higher and roughly of the same order of magnitude as the dissolved sulfate concentrations. The column was first equilibrated with at pH 3.71 without sulfate and subsequently infiltrated with a 1085 μM sulfate solution. After 6 pore volumes and complete breakthrough, the infiltrating solution was replaced with a solution without sulfate.

The general characteristics of the breakthrough curves (Figure 3) are similar to those of the experiments at pH 4.74. However, the separation of the sulfate infiltration and leaching curves into two separate fronts is now clearly visible (Figure 3A). The plateau between first and second fronts is much shorter than in the previous experiment, and complete breakthrough of sulfate is achieved within 4 pore volumes. After the infiltrating solution is changed to the one without sulfate, at 6 pore volumes, the sulfate concentration in the effluent drops sharply at the first front. This is immediately followed by a diffuse front during which the concentration slowly returns to zero.

In the pH breakthrough curves (Figure 3B), a significant increase of the pH occurs at the first infiltration front after 1.5 pore volumes. The pH remains at this value until the second front at 2.5 pore volumes, where it returns to the value of the input solution. After changing the input solution to the one without sulfate, at 6 pore volumes, the pH first drops rapidly by about half a unit at the first front, which is then immediately followed by a diffuse front where the pH slowly returns to the value of the input solution.

Again the simulations agree well with the experimental results. The sulfate concentrations are especially predicted accurately, but also the general features and positions of the pH breakthrough curves are predicted well. The main
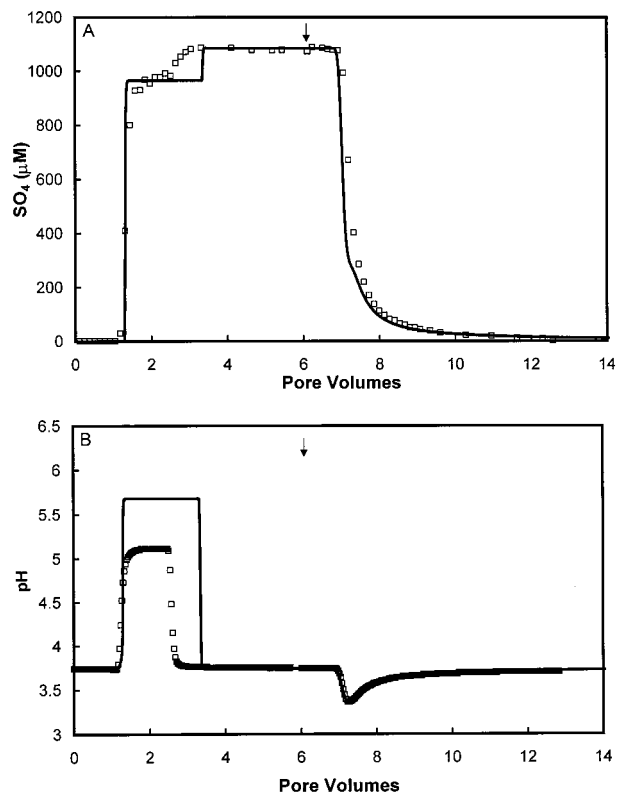
remaining discrepancy, as was the case with the experiments at pH 4.74, lies in the initial pH increase (between 1.5 and 4 pore volumes), which is overestimated by the model.

The same experiment was also carried out using a lower sulfate concentration of 384 μM in the input solution. The curves are very similar to those at the higher sulfate concentration The measured sulfate breakthrough curves again agrees very well with the predictions (Figure 4A). The pH curve shows the similar discrepancy in the height and length of the first plateau as was found in the previous experiments. The second, leaching, part of the pH curve however is predicted accurately (Figure 4B).

Changing Salt Concentration. The third experiment shows the effects of a change in salt level of the infiltrating solution on the leaching of protons and sulfate from the column. For this experiment, the column was initially equilibrated with a solution of 384 μM sulfate at pH 3.75 in 0.1 M NaCl. This column was then infiltrated with a similar solution but with a lower salt concentration of 0.01 M NaCl. After 6 pore volumes and complete breakthrough, the initial 0.01 M NaCl solution was applied again.

The system is now defined by three independent components. According to chromatographic theory, we can thus expect three separate fronts upon a step change in input concentration (*13*). In the sulfate breakthrough curve, we can see the first subfront after 1 pore volume as a decrease in the concentration (Figure 5A). This coincides with the unretarded front of the salt concentration. At the same time, the pH decreases to about 3.45 (Figure 5B). At the second subfront, which follows immediately, the sulfate concentration increases again to about 320 μM. At the same time, the pH increases sharply to about 4.2. At the third and final subfront, which occurs shortly before 2 pore volumes, both

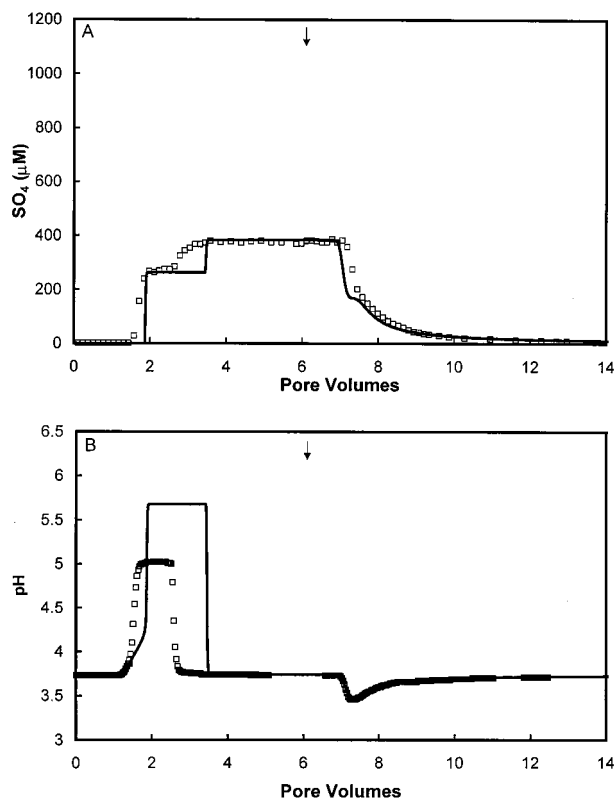FIGURE 4. Measured and simulated breakthrough curves for a column equilibrated without sulfate at pH 3.71, infiltrated with a 384 μM sulfate solution at pH 3.71. After 6 pore volumes, as indicated by the arrow, the infiltrating solution was replaced with a sulfate free solution of the same pH. (A) Total dissolved sulfate. (B) pH.

FIGURE 5. Measured and simulated breakthrough curves for a column equilibrated with 384 μM sulfate at pH 3.75 in 0.1 M NaCl. The column was infiltrated with a similar solution at 0.01 M NaCl. After 6 pore volumes, indicated by the arrow, the initial solution at 0.1 M NaCl was applied again. (A) Total dissolved sulfate. (B) pH.

the sulfate concentration and the pH return to their initial values.

After 6 pore volumes, the input solution is changed, and again three subfronts evolve. At the unretarded first subfront, the sulfate concentration now increases to almost double the initial value, and the pH increases slightly. In the second subfront, which follows immediately, the sulfate concentration decreases to about 500 μM, and the pH decreases to about 3.5. The third subfront is diffuse, and both the sulfate concentration and the pH return to their initial values.

The total amount of sulfate adsorbed and released by the column as a result of the changing salt concentrations is indicated by the surface area of the sulfate peaks. The good agreement between the predicted and the measured total surface areas indicates that the total amount of sulfate released and adsorbed by the column upon a change in salt concentration is predicted accurately. In this experiment, the breakthrough curves exhibit rapid changes in concentrations, which makes the results relatively sensitive for dispersion. It is interesting to note that the interaction between salt and sulfate concentrations is predicted indirectly by the adsorption model from the sulfate−proton and proton−salt interactions, and again the model appears to describe the general features of the curves very well.

Simultaneous Change in Salt and Sulfate Concentrations. The final experiment shows the effects of a simultaneous change in the salt and sulfate concentrations. In this case, the column was initially equilibrated with a solution at pH 3.75 in 0.1 M NaCl and subsequently infiltrated with 383 μM sulfate at pH 3.75 in 0.01 M NaCl. After complete breakthrough of this solution, at 6 pore volumes, the initial solution at 0.1 M NaCl without sulfate was applied again.

As this is again a three-component system, we can expect three fronts in the breakthrough curves (Figure 6). After 1
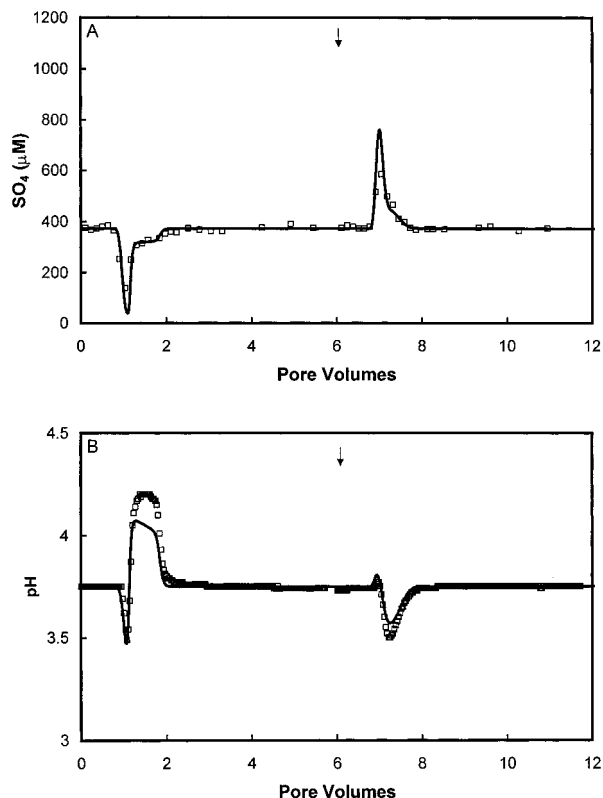
pore volume, at the unretarded front, the pH decreases to about 3.85, but no sulfate front is visible. This is because sulfate is retarded by adsorption and has not yet arrived at the end of the column after 1 pore volume. The first front is therefore effectively a salt−pH front. The second and third fronts are effectively proton−sulfate fronts, as the salt concentration does not change there. The second subfront starts shortly before 2 pore volumes and here the sulfate concentration increases to about 300 μM, while the pH increases to about 6. After 4 pore volumes, the pH and the sulfate concentrations return to the values of the input solution, thus forming the third subfront.

Upon changing the input solution after 8 pore volumes to the one at the higher salt level, the sulfate concentration sharply increases after 9 pore volumes to almost 1.5 times its initial value (Figure 7A). It then gradually decreases to zero with a diffuse front, which is not fully completed after 15 pore volumes. At the end of the experiment, about 30% of the sulfate is still present in the column. This diffuse front is actually composed of the second and third subfronts, and again the individual subfronts are easier to identify in the pH curve (Figure 7B). Here, we can see an unretarded front after 9 pore volumes, where the pH increases slightly, immediately followed by the second subfront where the pH decreases about 3.45 and the third, diffuse front where the pH slowly returns to its initial value. In the pH breakthrough curve, a decrease in pH after 1 pore volume is visible, which coincides with breakthrough of the unretarded salt front. At this front, there is no change in composition of the solid phase, so no ad- or desorption of protons or sulfate takes place (which would result in retardation). The pH and sulfate concentrations are therefore forced to change to a composition in equilibrium with the amounts of adsorbed sulfate and protons at the lower salt concentration of 0.01 M NaCl.
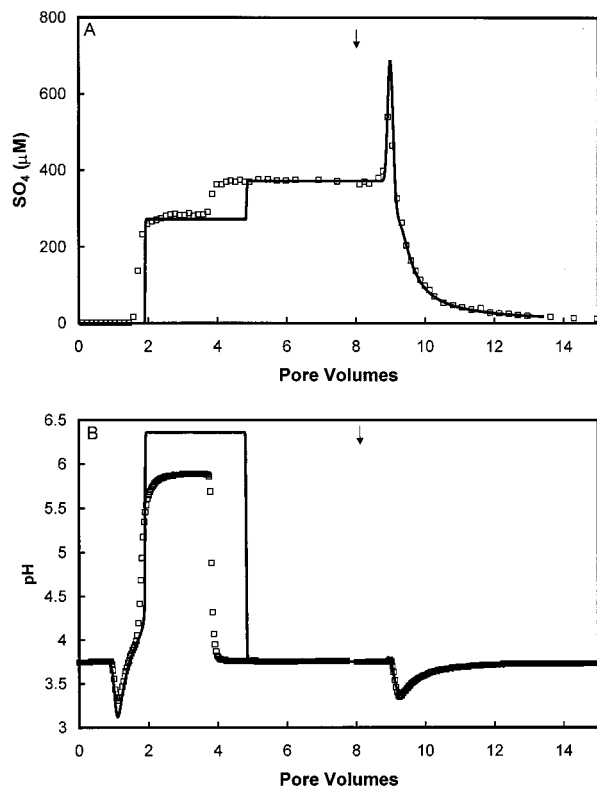
FIGURE 6. Measured and simulated breakthrough curves for a column equilibrated with a sulfate-free solution at pH 3.75 in 0.1 M NaCl, infiltrated with a solution containing 384 μM sulfate at pH 3.75 in 0.01 M NaCl. After 6 pore volumes, indicated by the arrow, the initial solution at 0.1 M NaCl without sulfate is applied again. (A) Total dissolved sulfate. (B) pH.
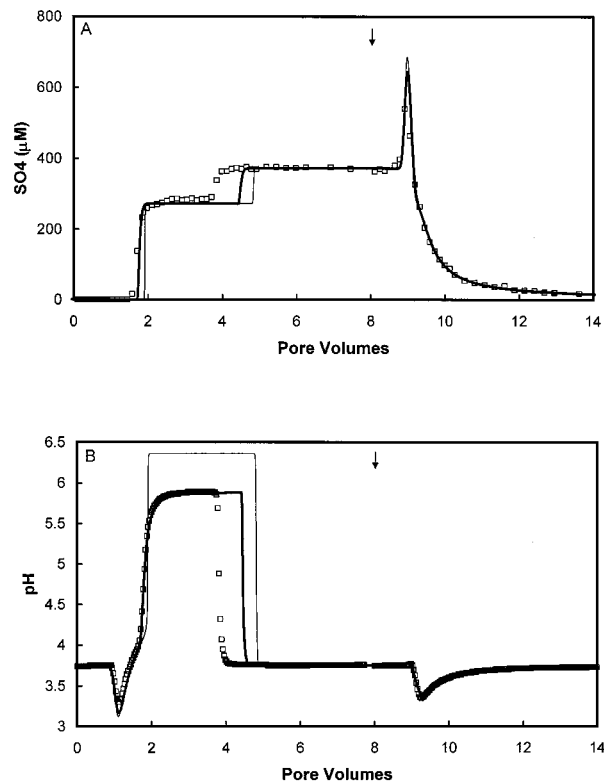
FIGURE 7. Measured and simulate breakthrough for a system identical to that of Figure 6, but now taking into account in the simulations a small amount of sulfate initially present in the column and extra dispersion caused by the pH measurement cell. The thin lines indicate the original calculations of Figure 6. (A) Total dissolved sulfate. (B) pH.

The predicted pH and sulfate breakthrough curves agree very well with the measurements. The sulfate breakthrough curve is described extremely well. The largest remaining discrepancy exists again in the height and length of the pH plateau between 2 and 4 pore volumes, which is underestimated by the model.

Possible Causes for Remaining Differences between Measured and Predicted Breakthrough Curves. Comparison of all the experimental results with the simulations shows that the predictions are relatively accurate. Nevertheless, there still are some remaining discrepancies for which there are several possible causes.

Sorption Properties of the Goethite. The goethite used in the column here was not the same material as was used to derive the parameters for the proton and sulfate adsorption model. The goethite used here has a reported PZC of 7.2 and a specific surface area of 24 m^2/g (3), whereas for the goethite used to derive the adsorption model, these values are 9.2 and 94 m^2/g respectively (5). Differences between these materials in adsorption behavior per unit surface area is likely to result in differences between the predicted and measured breakthrough curves.

Sulfate Concentrations during Transport. During the transport calculations, the adsorption model is used at sulfate concentrations that are significantly lower than those originally used to determine the sulfate adsorption parameters. These extrapolations introduce an element of uncertainty to the transport calculations and may also result in incorrect transport predictions. However, the used adsorption model appears to extrapolate these conditions well.

Initial Sulfate Contents of Column. A further cause for differences between model and experiment is the amount of sulfate initially present in a column before an experiment is

started. In the calculations for experiments 1, 2, and 4, this amount was assumed to be zero, but, in reality, sulfate was removed from the columns by flushing with a clean solution at the required pH. However, as demonstrated by the long diffuse sulfate "tails" in the breakthrough curves of experiments 1, 2, and 4, complete removal will be virtually impossible due to the strongly nonlinear adsorption behavior of sulfate.

Dead Volume of pH Measurement Cell. Dispersion can affect the breakthrough curves, especially the sharp peaks in experiments 3 and 4. It is therefore important to use the correct dispersivity in the simulations. The dispersivity of the experimental column is determined by measuring the dispersion of a chloride pulse. However, this procedure does not take into account the additional dispersion in the pH measurement cell, which is replaced by the chloride detector. The overall dispersion observed in the pH measurements thus is the sum of the dispersion taking place in the reactive part of the column and the dispersion in the pH cell and tubing after the column. Other possible sources for additional dispersion for reactive solutes could be adsorption kinetics or spatial heterogeneity in chemical properties of the adsorbent.

The exact effect of the first two factors is difficult to assess without conducting additional experiments. The effects of the latter two however can be estimated by taking them into account in the simulations. Therefore, we repeated the simulations with the following changes. Instead of starting a simulation with a completely clean column, we assumed that the column was flushed for 30 pore volumes with a clean solution of the correct pH. This agreed with the actual procedure followed in the experiments. Furthermore, the effect of dead volume in the pH cell and tubing was simulated

with a completely mixed volume (6.7% reactive column volume) at the end of the column. The results of these simulations are shown Figure 7.

It is clear that these changes affect the results significantly. A small amount of sulfate initially present in the column reduces the extra amount of sulfate that adsorbs upon infiltration with the sulfate solution during the experiment, resulting in slightly faster initial breakthrough of sulfate. Also, the amount of adsorbing protons is reduced, which results in a smaller increase in pH and a lower plateau between the first and the second fronts. Only the infiltration part of the curves is affected because, after complete breakthrough of the first solution, the situation in the column is similar to the previous simulation. The extra dispersion in the pH measurement cell causes the asymmetric rounding of the edges of the first pH fronts, which are now very similar in shape to the experimental curves.

Although the overall effect of these modifications is that the simulations agree much better with the experiments, the aim of this exercise is not to obtain perfect simulations. It is much more useful to demonstrate the sensitivity of the system for small uncertainties in the initial chemical conditions. This is the case for the synthetic system studied here but will be even more important when studying real systems. In soils, many different substances are present, and surfaces are exposed to many different adsorbates. Strongly adsorbing substances, such as phosphate, can significantly affect adsorption and transport behavior of other ions already at low dissolved concentrations. Thus, even if the used adsorption/transport models are in principle relatively accurate and able to describe behavior in pure systems, simulating transport in soil systems requires accurate data on the initial chemical conditions.

Acknowledgments

Supporting Information Available

A description of the model and experimental section including 5 figures and captions (11 pages). This material is available free of charge via the Internet at http://pubs.acs.org.

Literature Cited

(1) Scheidegger, A. M.; Bürgisser, A. S.; Borkovec, M.; Sticher, H.; Meeussen, J. C. L.; van Riemsdijk, W. H. *Water Resour. Res.* **1994**, *30*, 2937.

(2) Meeussen, J. C. L.; Scheidegger, A. M.; Hiemstra, T.; van Riemsdijk, W. H.; Borkovec, M. *Environ. Sci. Technol.* **1996**, *30*, 481.

(3) Scheidegger, A. M.; Borkovec, M.; Sticher, H. *Geoderma* **1993**, *58*, 43.

(4) Hiemstra, T.; van Riemsdijk, W. H.; Bolt, G. H. *J. Colloid Interface Sci.* **1989**, *133*, 105.

(5) Hiemstra, T.; van Riemsdijk, W. H. *J. Colloid Interface Sci.* **1996**, *179*, 488.

(6) Geelhoed, J. S.; Hiemstra, T.; van Riemsdijk, W. H. *Geochim. Cosmochim. Acta* **1997**, *61*, 2389.

(7) Jauzein, M.; Andre, C.; Margrita, R.; Sardin; M. Schweich, D. *Geoderma* **1989**, *44*, 95.

(8) Meeussen, J. C. L.; Meeussen, V. C. S.; Lumsdon, D. G. In *Hydroinformatics'96;* Mueller, A., Ed.; Balkema: Rotterdam, 1997; Vol. 2, pp 557−564.

(9) Herzer, J.; Kinzelbach, W. *Geoderma* **1989**, *44*, 115.

(10) Schweich, D.; Sardin, M.; Jauzein, M. *Water Resour. Res.* **1993**, *29*, 723.

(11) Keizer, M. G.; van Riemsdijk, W. H. *Ecosat, a Computer Program for the Calculation of Chemical Speciation and Transport in Soil−Water Systems*; Wageningen Agricultural University: Wageningen, The Netherlands, 1995.

(12) Lindsay, W. L. *Chemical Equilibria in Soils*; John Wiley and Sons: New York, 1979.

(13) Helfferich, F. J.; Klein, G. *Multicomponent Chromatography Theory of Interference*; Marcel Dekker: New York, 1970.

(14) Engesgaard, P.; Christensen, T. H. *Nord. Hydrol.* **1988**, *19*, 188.

(15) Cederberg, A. S.; Street, R. L.; Leckie, J. O. *Water Resour. Res.* **1985**, *21*, 1095.